BULLETIN OF THE POLISH ACADEMY OF SCIENCES
TECHNICAL SCIENCES, Vol. 69(6), 2021, Article number: e139316
DOI: 10.24425/bpasts.2021.139316

State-of-the-art rotordynamic analyses of pumps

Frédéric GAULARD*, Joachim SCHMIED, and Andreas FUCHS

Delta JS AG, Technoparkstrasse 1, 8005 Zürich, Switzerland

Abstract. State-of-the-art analyses for the rotordynamic assessment of pumps and specific requirements for the simulation tools are described. Examples are a horizontal multistage pump with two fluid film bearings in atmospheric pressure, a horizontal submerged multistage pump with many bearings, and a submerged vertical single-stage pump with water-lubricated bearings. The rotor of the horizontal pump on two bearings is statically overdetermined by the seals and the static bearing forces depend on the deflection in the seals and the bearings. The nonlinear force-displacement relation in the bearings is considered in this paper. The stability of pumps is assessed by Campbell diagrams considering linear seal and bearing properties. Cylindrical bearings can have a destabilizing effect in the case of low loads as in the examples of the submerged pumps. For the pump with many bearings, the influence of the bearing ambient pressure and the bearing specific load on the stability is analyzed. For the vertical pump, the limit cycle, i.e. the vibration level of stabilization, is determined with a nonlinear analysis. All examples have a practical background from engineering work, although they do not exactly correspond to real cases. Analyses were performed with the rotordynamic software MADYN 2000.

Key words: rotordynamics; lateral analysis; pumps; fluid-film bearings; pump seals; nonlinear analysis.

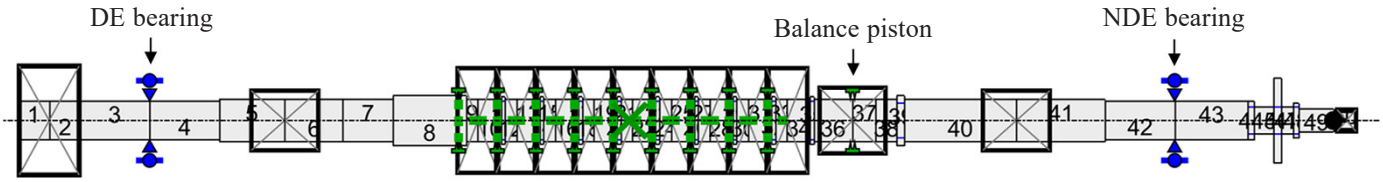

Fig. 1. Horizontal multistage pump on two bearings at atmospheric pressure

1. INTRODUCTION

Fluid-rotor interaction plays a big role in the rotordynamics of pumps. The forces in small clearances, i.e. at the seals and bearings, have the largest impact. The seal forces can have a destabilizing effect, but also a stiffening effect (Lomakin) and thus contribute to carrying the weight load.

There is a long history of research on the impact of seals and complete impellers in rotordynamics. They are typically considered by rotordynamic stiffness, damping, and mass coefficients. A good summary of activities can be found in the book of Dara Childs [1].

Special requirements for rotordynamic analyses due to the seals are described in this paper for the example of a horizontal pump in atmospheric pressure.

Fluid film bearings have a long history in research as well. Famous researchers are Glienicke [2] and Lund [3]. In 1994, the 2-phase flow was introduced [4] as a new cavitation model. It facilitates a better description of the properties of a mixture of oil and gas as well as considering the influence of elevated environmental pressure on cavitation. At high pressure, it is suppressed completely (so-called Sommerfeld boundary condition).

In submerged pumps, the bearings are lubricated by the process fluid and are in a pressurized environment. Therefore, the suppression of cavitation plays a big role in these machines. This leads to a surprising behavior, different from the normal behavior of bearings in the atmospheric pressure environment. Many engineers are not aware of this since it has not been described in textbooks so far. The description of a submerged pump exemplifies this behavior.

The behavior of nonlinear fluid film bearing is an issue for vertical pumps, the third example in this paper. They are typically linearly unstable. A nonlinear analysis facilitates assessing the vibration level by calculating the limit cycle.

2. HORIZONTAL MULTISTAGE PUMP WITH TWO BEARINGS AT ATMOSPHERIC PRESSURE

2.1. Description of the model

The model of the centrifugal pump is shown in Fig. 1. The rotor has a total length of 1730 mm and a bearing span of 1330 mm. The mass of the rotor is 52 kg, with a nominal speed of 9000 rpm. It is supported on two tilting-pad bearings with a diameter of 50 mm and a clearance of 2.0‰, which are lubri-

*e-mail: contact@delta-js.ch

Manuscript submitted 2021-03-31, revised 2021-07-23, initially accepted for publication 2021-09-02, published in December 2021

cated with an oil-type ISO VG46 with an inlet temperature of 50°C. The bearings are analyzed as described in [5] with consideration of the 3D distribution of the temperature and viscosity in the fluid film, the turbulence in the fluid film, and the thermo-elastic deformation of the shaft and pads.

The seals at the impeller shrouds and hubs, as well as the balance piston seal, are included in the model. The impeller seals are plain annular seals; the balance piston seal is serrated.

The seals are analyzed with the specialized CFD program SEAL 2D/3D, which was originally developed by Nordmann et al. (see [6]), further improved for industrial use, and integrated into MADYN 2000 (see [7]). The code solves the Navier-Stokes equations with the finite difference method. For the balance piston, the radial and tangential forces as a function of the precession frequency at nominal speed are shown in Fig. 2. The calculated points are shown with "Xs". The speed-dependent linear coefficients, including mass coefficients, are determined by curve fitting (solid lines).

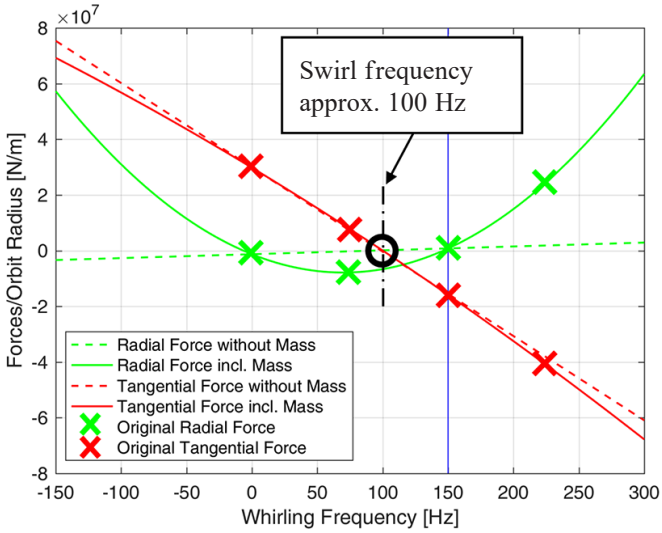

Fig. 2. Balance piston seal, forces vs. whirling frequency

2.2. Static analysis

The static analysis yields the bearing loads, which are needed to determine the load and speed-dependent bearing characteristics. The seal forces influence the static equilibrium of the rotor. With a total of 18 seals and 2 bearings, the shaft is statically overdetermined. The relation between the bearing force and displacement in fluid film bearings is nonlinear. Therefore, a nonlinear static analysis is required. The seal characteristics are assumed as linear since they have larger clearance and cavities.

On some pumps, the bearing housings are raised relative to the pump casing to reduce the static shaft eccentricity at the seal locations. This can be considered in the analysis. In the present example, the seal clearances are sufficiently high to avoid rubbing, and the bearing housings were not lifted.

Due to the speed dependence of the seals and bearings, the static analysis must be conducted for the whole speed range of interest. The analysis starts with rigid supports instead of the actual bearings (no compliance due to the fluid film), which yields a first estimate of the bearing forces. The journal position in the bearing caused by the bearing force is then calculated yielding a new bearing force and a new position. During each iteration step, the bearing code is called with the relevant force and returns the journal position. The iteration stops when the change of force and position in an iteration step is sufficiently small.

The shaft displacements at a nominal speed from two different static analyses are shown in Fig. 3. The plot on the top is the result of an analysis where the bearings are modelled as rigid supports and the seal forces are not considered. For the bottom plot, the analysis was conducted with consideration of the nonlinear bearing characteristics and the seal forces. The

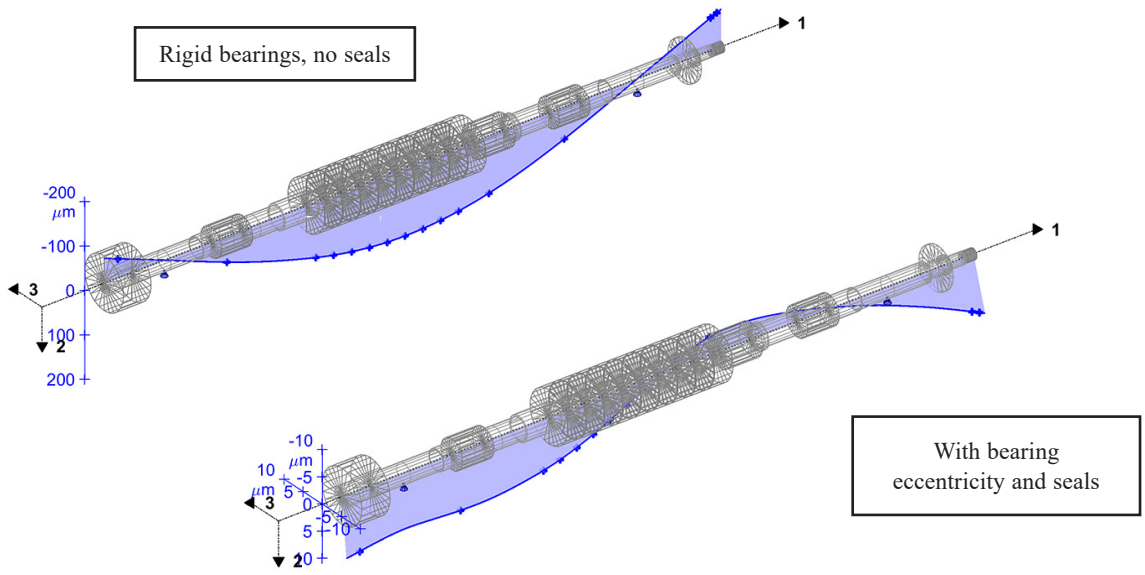

Fig. 3. Results of the static analysis – Shaft displacement at 9000 rpm

influence of the seals is visible, notably at the balance piston seal, where the shaft is significantly lifted.

Plots of the shaft forces can be found in Fig. 4. When the seal forces are considered, the bearing loads are much lower.

The speed-dependent bearing forces at the non-drive end bearing (NDE bearing) can be seen in the upper left quadrant of Fig. 5. The corresponding displacements are shown in the lower-left quadrant. The bearing coefficients can be seen on the right of the figure.

2.3. Campbell diagram

The Campbell diagram is calculated with the speed-dependent bearing loads and speed-dependent linear coefficients for the bearings and the seals, as shown in Fig. 6 together with the mode shapes at the critical speeds.

The assessment of the eigenvalues at nominal speed according to API 610 can be found in Fig. 7 (see [8]). The modes are well damped and smooth operation is expected for this pump.

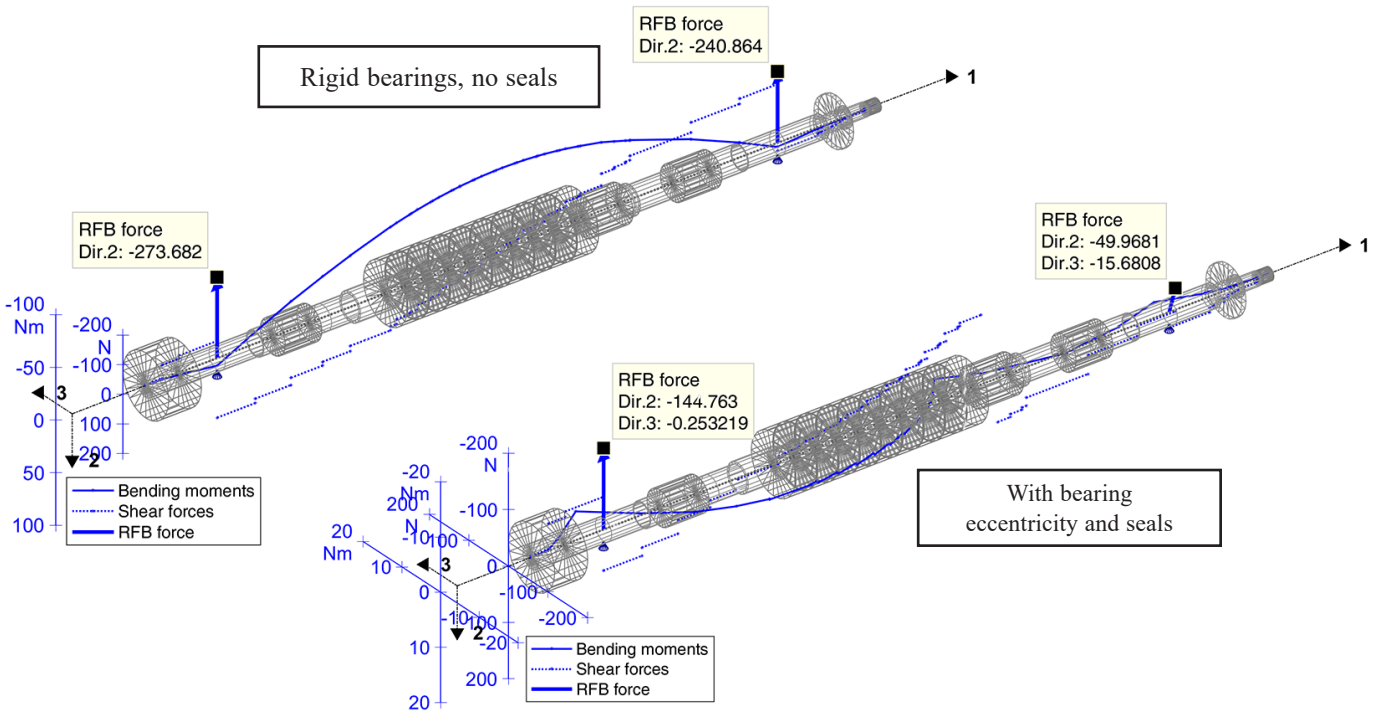

Fig. 4. Results of the static analysis – shaft forces at 9000 rpm

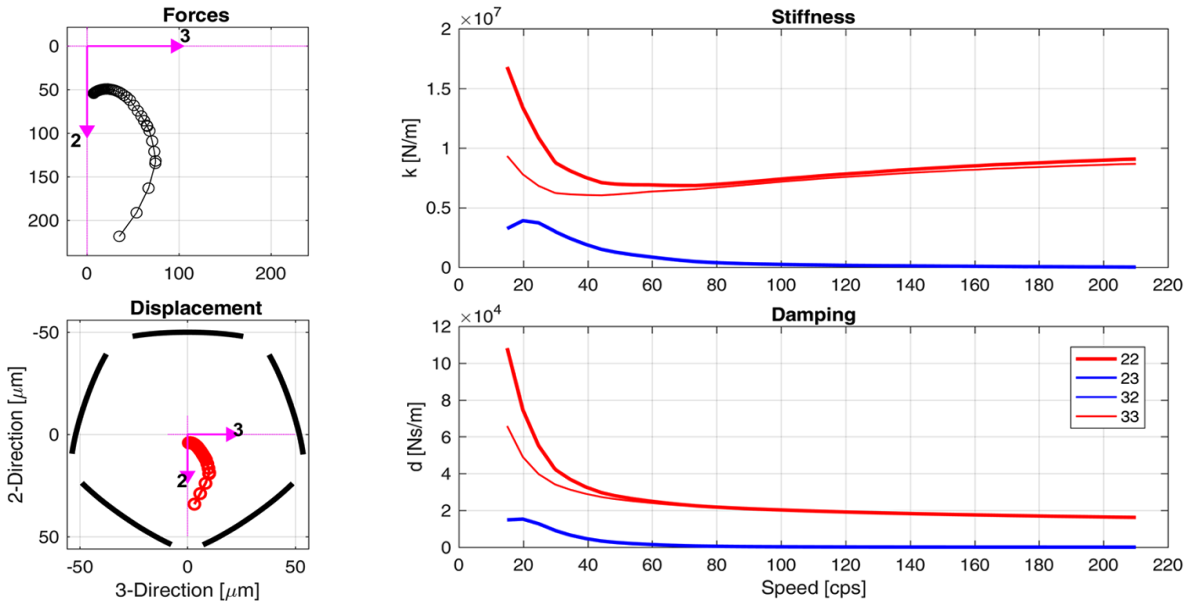

Fig. 5. NDE bearing – results of the bearing analysis and linear coefficients

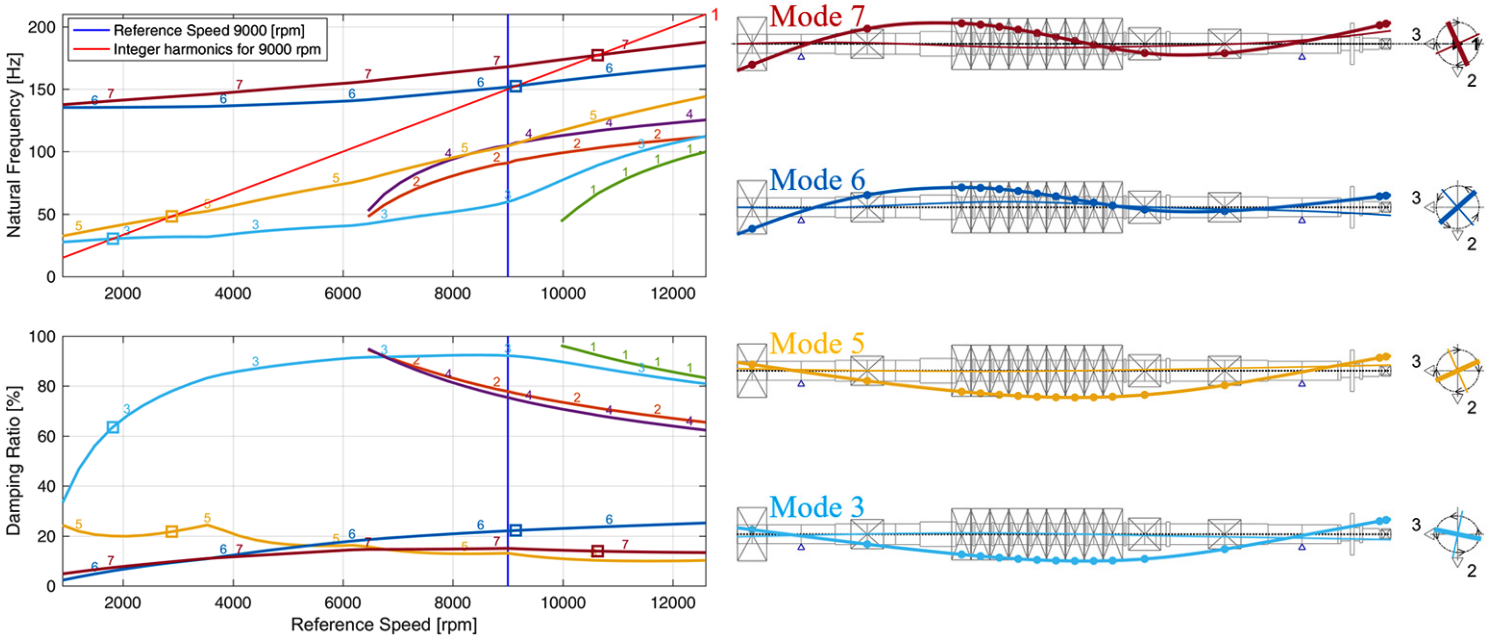

Fig. 6. Campbell diagram and critical modes

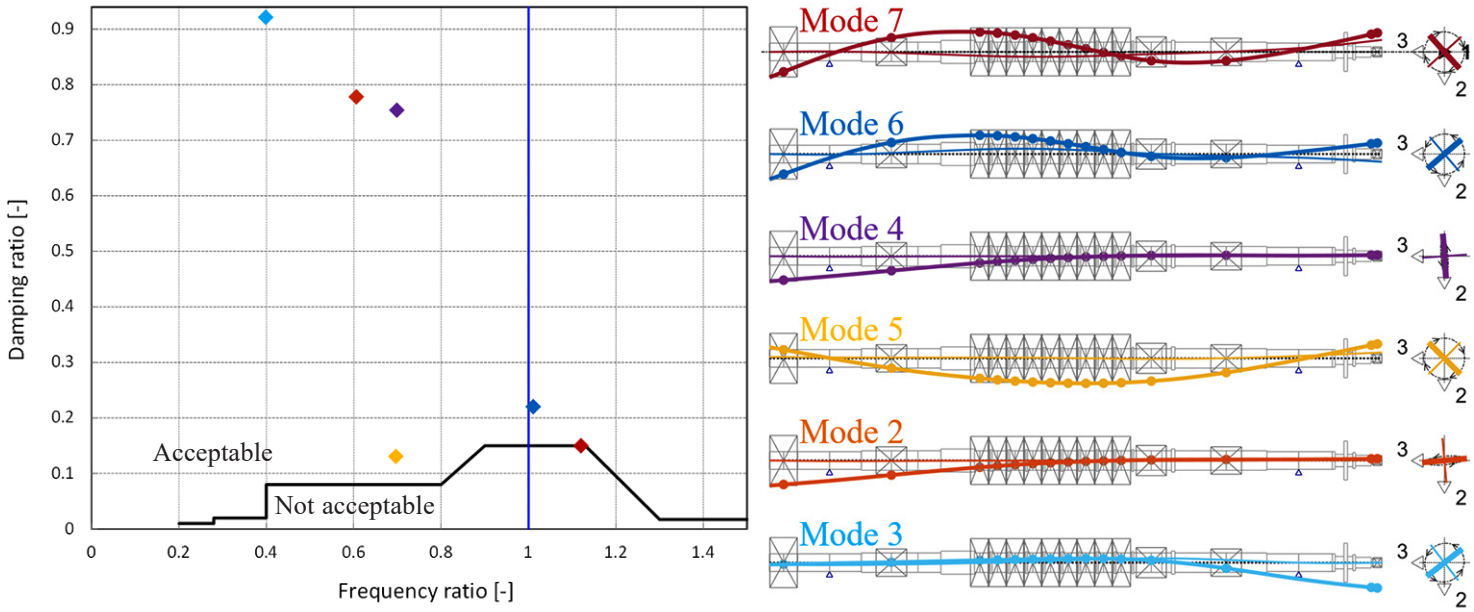

Fig. 7. Assessment of the eigenvalues according to API 610 and mode shapes at 9000 rpm

3. SUBMERGED HORIZONTAL MULTISTAGE PUMP WITH MANY BEARINGS

Submerged electrical pumps can have many stages and typically have very elastic shafts. For this reason, they have many bearings. In this section of the paper, we look at a sector with a few stages of such a pump to demonstrate some effects, which can occur in such a pump. The whole rotor in such a pump is surrounded by crude oil, which is also used as a lubricant for the bearings. In our example, the viscosity is 0.1 Pa · s at 85°C and the density is 920 kg/m^3.

3.1. Description of the model

A plot of the analyzed shaft sector can be seen in Fig. 8. The shaft diameter is 36 mm; the nominal speed is 4600 rpm. The rotor was cut midway between two bearings. At the end of this shaft sector, the added masses used to model the impellers have half the mass of the actual impellers. Quasi-rigid bending springs have been added at the ends of the rotor to calculate the correct bearing loads in the static analysis. Due to the relatively small impeller head, the seal forces are rather small and therefore negligible.

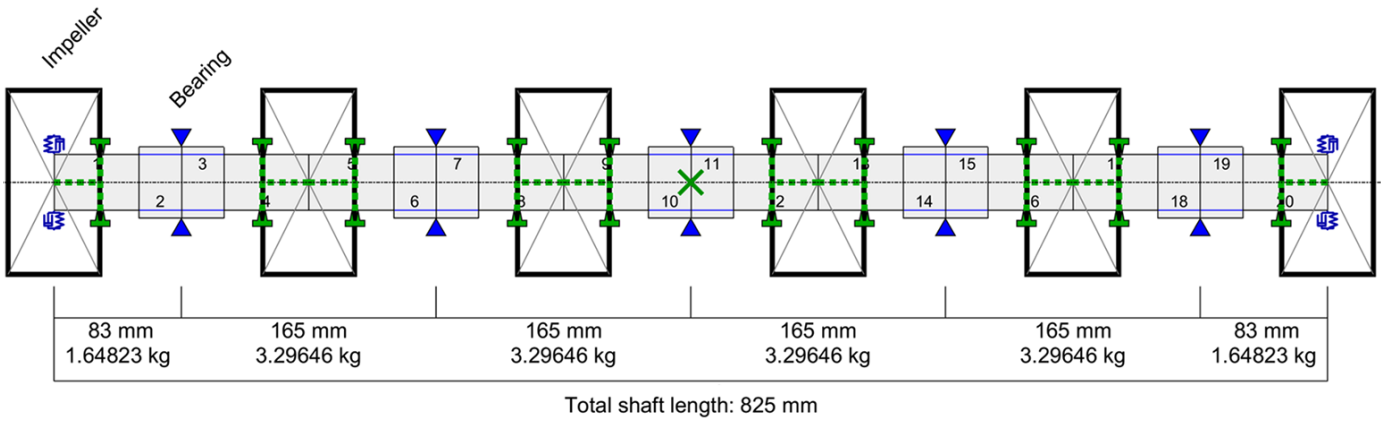

Fig. 8. Horizontal multistage pump with many pressurised bearings

The bearings are closed cylindrical bearings (i.e. cylindrical bearings with one continuous sector between 0° and 360°) with axial oil inlet (pressure difference across the bearing of 2.5 bar). The relative bearing clearance is 3‰. The shaft journal is cylindrical, without any axial or helicoidal groove. The bearings are lubricated with the pumped fluid and the ambient pressure increases with each stage (between 107.5 bar and 120 bar for the present example). The static analysis with a weight load was conducted on rigid supports, which is an acceptable simplification for such a flexible rotor supported on so many bearings. The bearing specific load is approximately 0.2 bar. The bearings were analyzed with consideration of the 2-phase cavitation model described in [5].

Results for the bearing at an ambient pressure of 107.5 bar are shown in Fig. 9. Typical of a closed cylindrical bearing, the displacement of the journal is perpendicular to the load. The direct stiffness is very small and the cross-coupling stiffness high, which contributes to destabilizing the rotor.

3.2. Campbell diagram

The Campbell diagram can be seen in Fig. 10. The first mode is the forward whirling parallel mode of the shaft. The other modes are the forward bending modes of the rotor with increasing order and frequency. All modes have circular orbits.

For all modes, the natural frequency is approximately half of the rotating speed, which corresponds to the oil-whirling

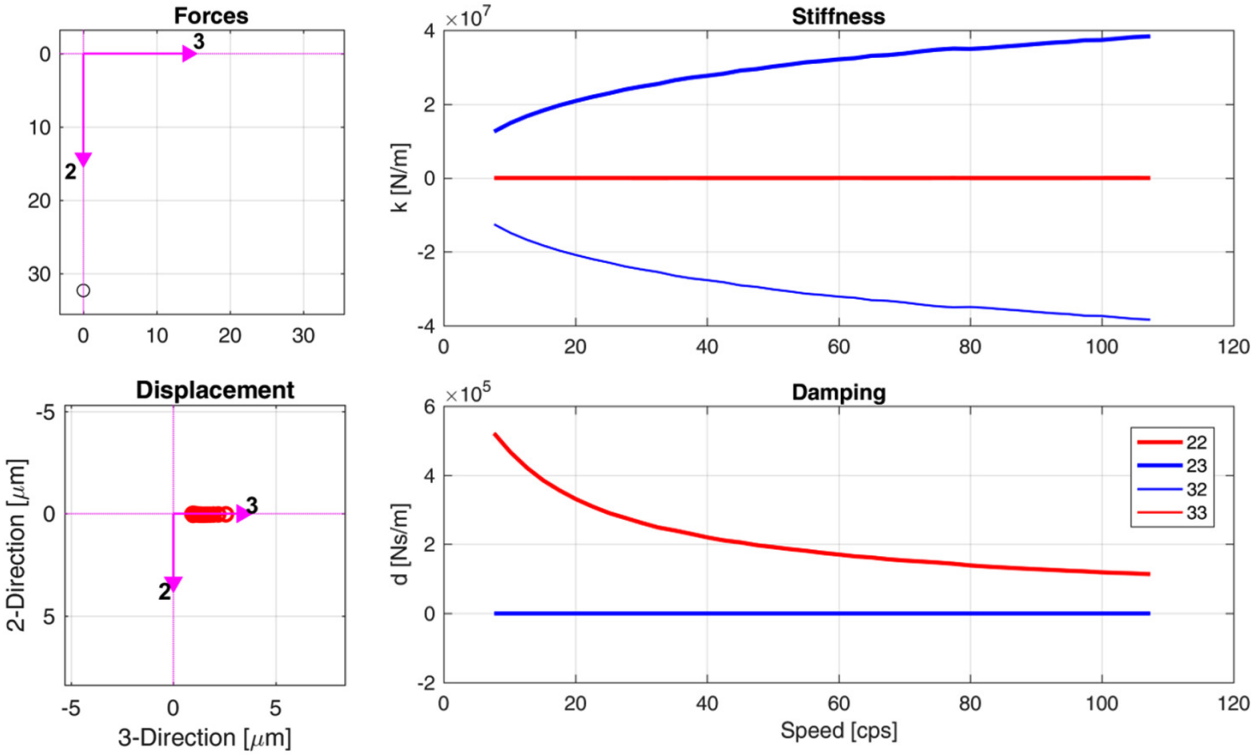

Fig. 9. Results of the bearing analysis and linear coefficients

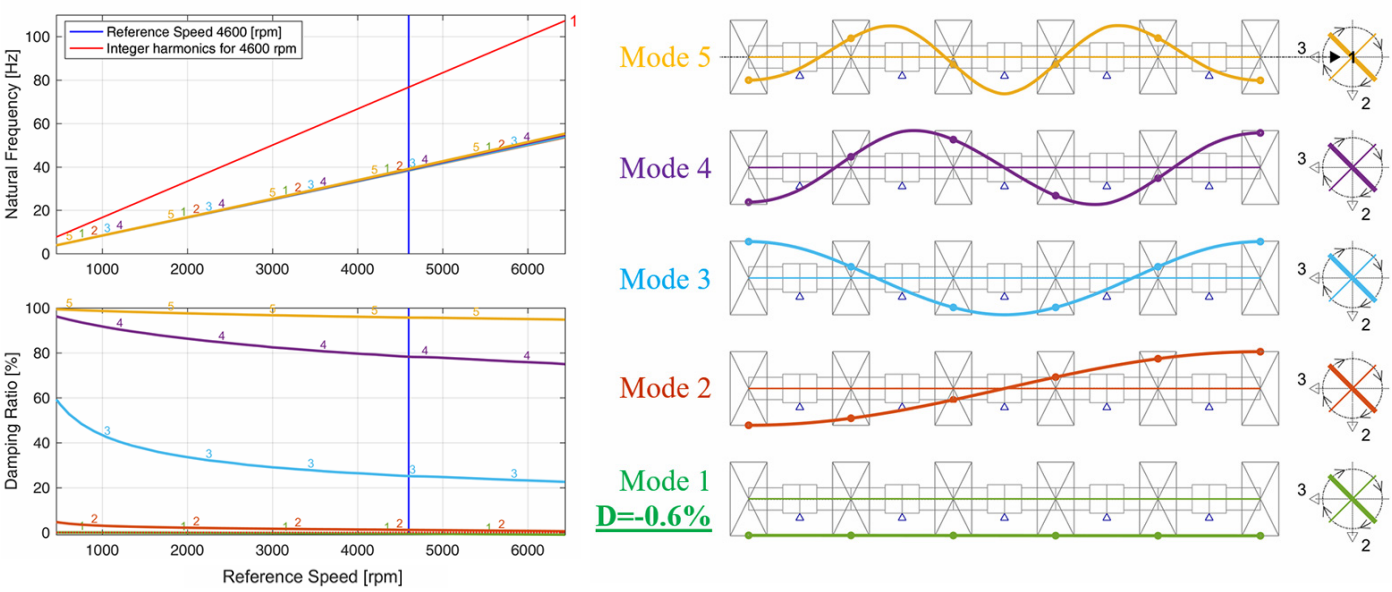

Fig. 10. Campbell diagram and mode shapes at 4600 rpm

frequency. The damping ratio of the 1st mode is slightly negative (i.e. the mode is unstable). The other modes have positive damping ratios. Modes 3 and higher have high damping ratios.

3.3. Influence of the bearing ambient pressure when the bearing specific load is constant

In this section, the influence of the ambient pressure on the eigenvalues at nominal speed was analyzed. The bearing specific load is kept constant at 0.2 bar. The ambient pressure is the same for all bearings and is increased from 1 bar (atmospheric pressure) up to 100 bar.

The natural frequencies do not change much with the ambient pressure, whereas it has more influence on the damping ratios. The damping ratios of modes 1 and 2 as a function of the ambient pressure are shown in Fig. 11. Between 1 bar and approximately 7 bar, the damping ratios decrease with the increasing ambient pressure. Beyond 7 bar, the influence of the ambient pressure is small.

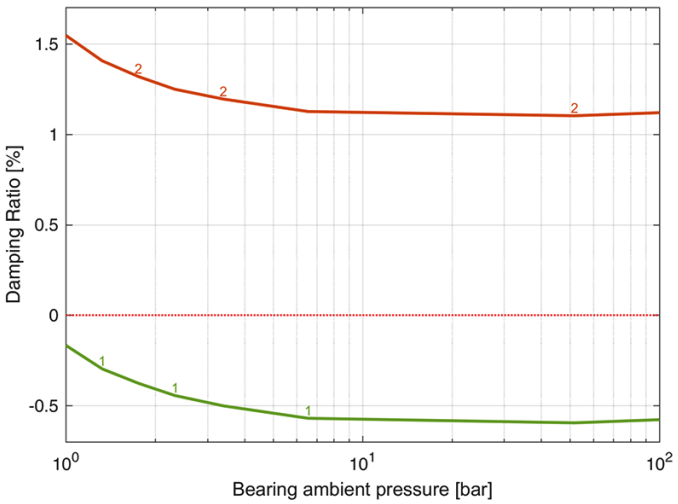

Fig. 11. Damping ratio of the 1st and 2nd mode at 4600 rpm vs. bearing ambient pressure

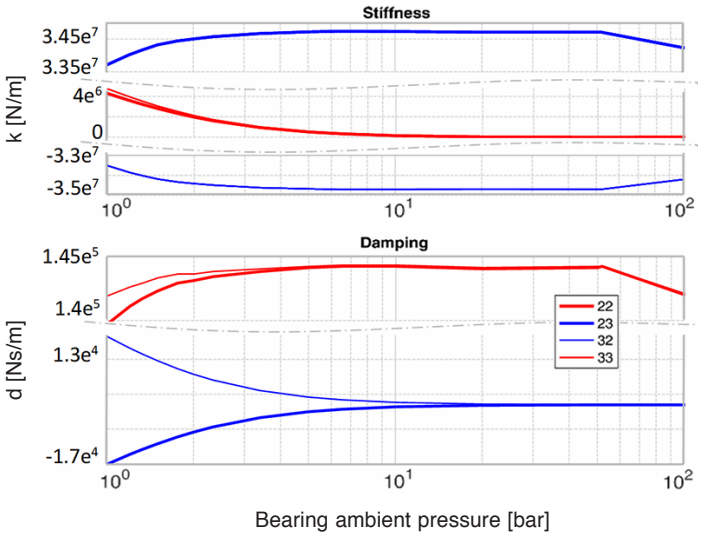

Fig. 12. Bearing coefficients vs. ambient pressure

The bearing coefficients at nominal speed as a function of the ambient pressure can be seen in Fig. 12. The direct stiffness coefficients and the cross-coupling damping coefficients cause radial forces to decrease with the ambient pressure. At the same time, the cross-coupling stiffness, which tends to destabilize the rotor, increases. The combination of both phenomena contributes to the decrease in the damping ratio of the modes when the ambient pressure increases.

3.4. Influence of the bearing specific load

In this section, the influence of the specific bearing load is shown at a constant ambient pressure between 107.5 bar and

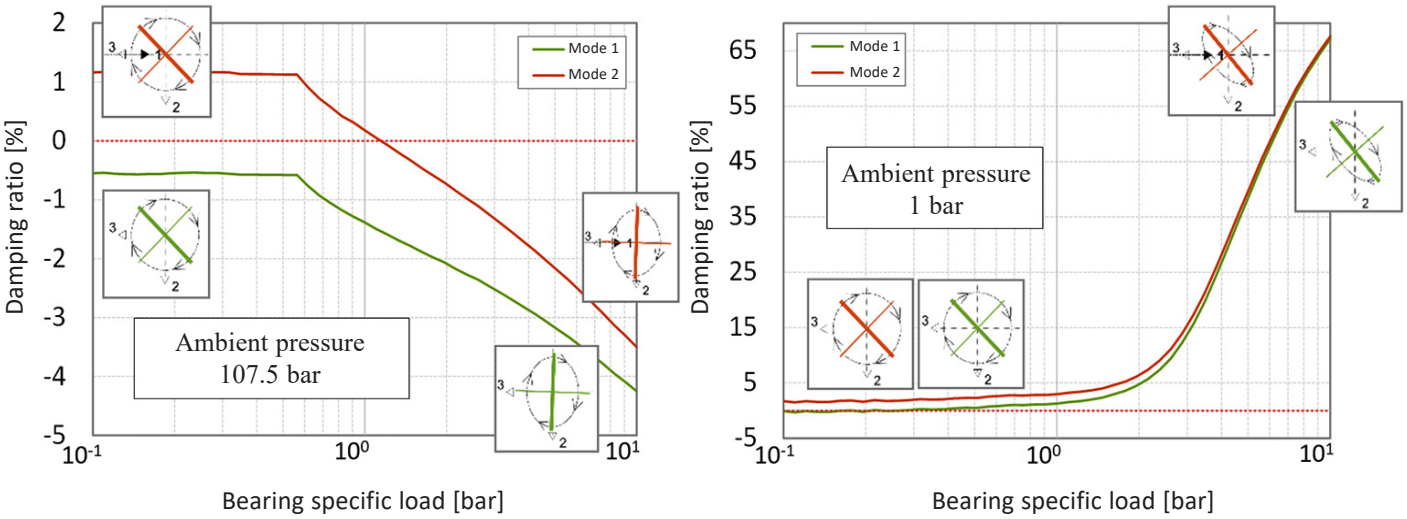

Fig. 13. Damping ratio of the 1st and 2nd mode vs. bearing specific load

120 bar. The damping ratio of the 1st and 2nd modes as a function of the bearing specific load can be seen in Fig. 13. For comparison, results with an ambient pressure of 1 bar are shown as well. The actual bearing specific load could be increased, for example, by reducing the number of bearings, reducing the diameter or the width of the bearings, or by applying adequate misalignment between the bearings.

When the bearings are at atmospheric pressure, the damping ratios increase with the specific load slowly up to 2.5 bar of specific load, and then more rapidly. They can even reach very high values for bearing loads around 10 bar. This behavior is expected for rotors on fluid film bearings and is reported in many textbooks.

With pressurized bearings, the damping ratio stays constant if the bearing load is lower than 0.56 bar and then decreases, which is surprising considering the usual behavior of rotors on fluid film bearings.

The rotordynamic stiffness and damping coefficients for the two cases are shown in Fig. 14. It is evident that the pressurized bearing with an increasing bearing load continues to behave like an unloaded cylindrical bearing. The direct stiffness remains small and the destabilizing skew-symmetric cross-coupling stiffnesses are large and increase with the bearing load. Direct damping is also increasing with the load. In contrast to this, the direct stiffness increases for the bearing in atmospheric pressure, and the stiffness matrix turns into an asymmetric but no longer skew-symmetric matrix.

The behavior can be explained by looking at the pressure distribution and static deflection of the shaft for the two cases: pressurized bearing and bearing in atmospheric pressure.

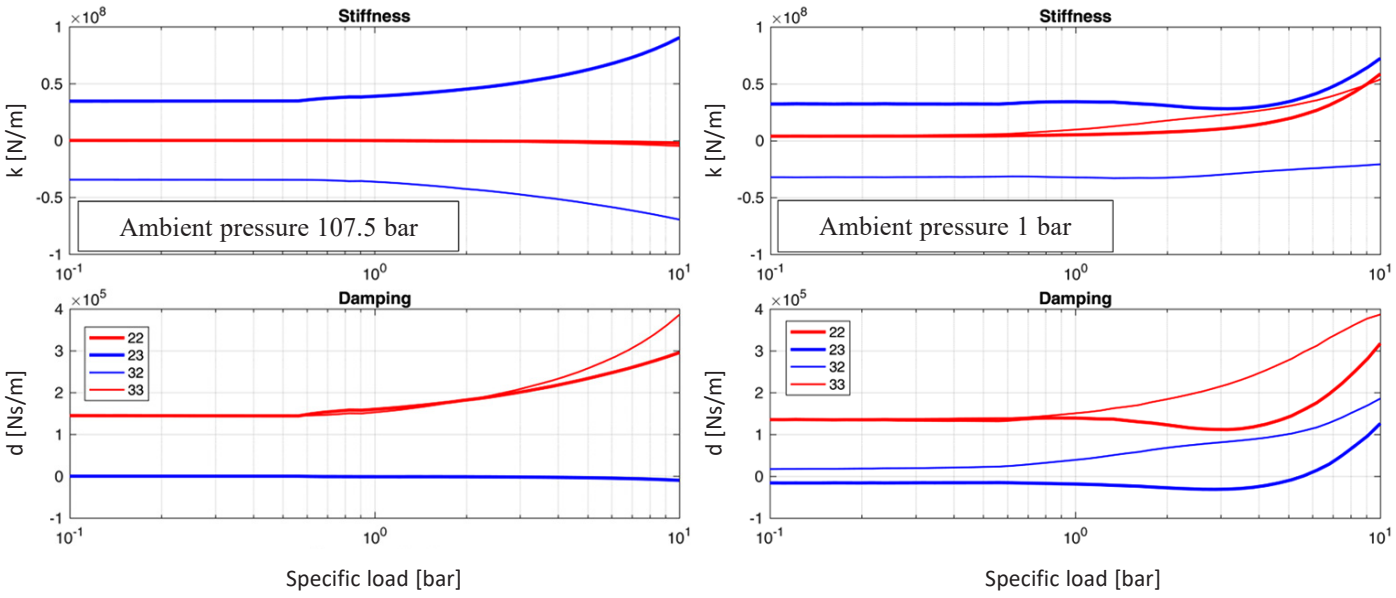

Fig. 14. Bearing coefficients vs. bearing specific load

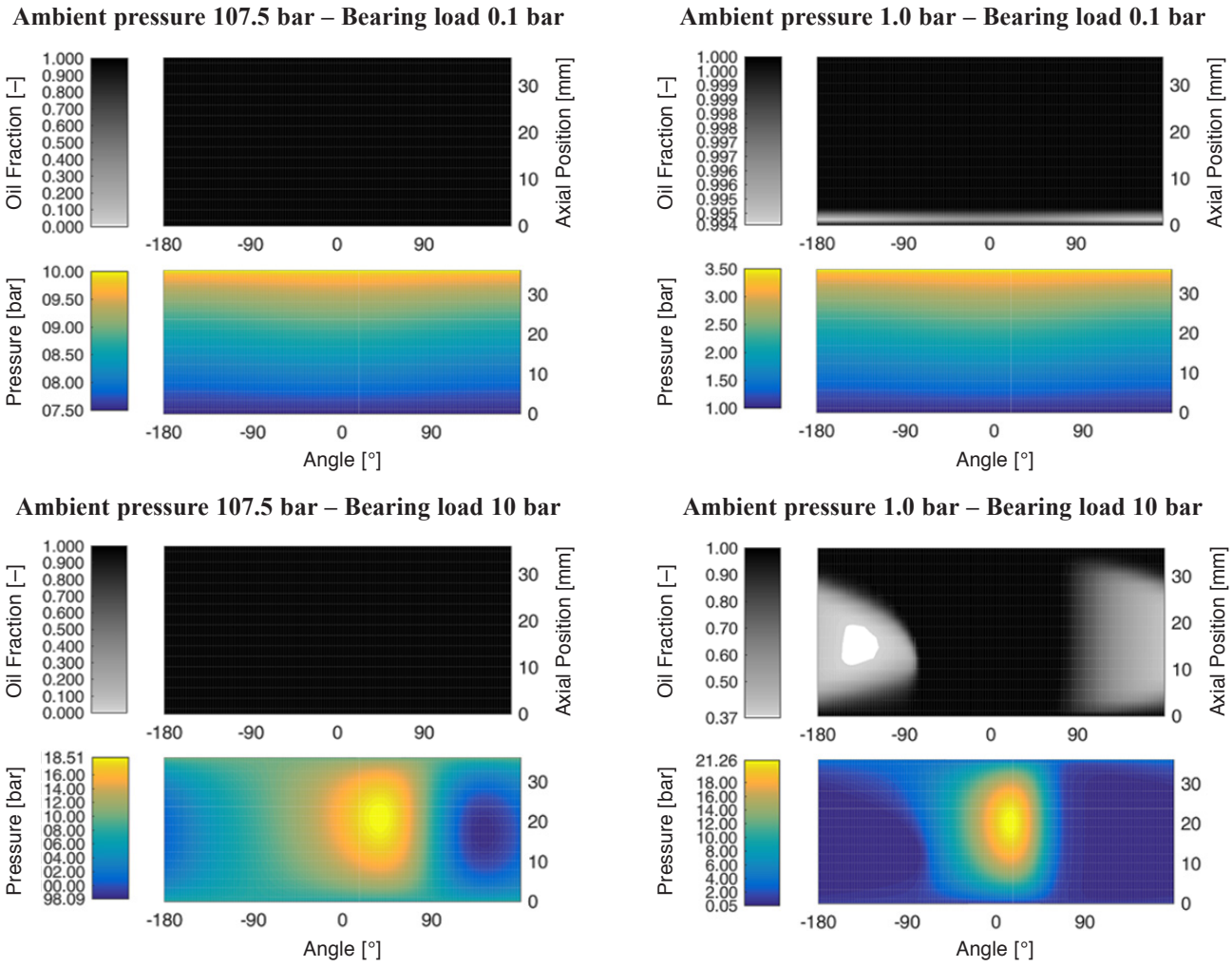

Fig. 15. Cavitation area and pressure distribution in the bearing oil film

The pressure distribution and the oil ratio in the fluid film are shown for the two cases in Fig. 15. The axial pressure difference is 2.5 bar. The results are represented in 2D fields where the x-axis is the circumferential angle (0° is at the bottom of the bearing, i.e. in direction 2 of Fig. 16) and the y-axis is the axial coordinate. For a given location, an oil ratio of 1.0 means that the volume is filled with oil; an oil ratio equal to 0 means that the volume is filled with air.

With a low specific bearing load of 0.1 bar, the pressure distributions are rather similar for the two cases. There is no

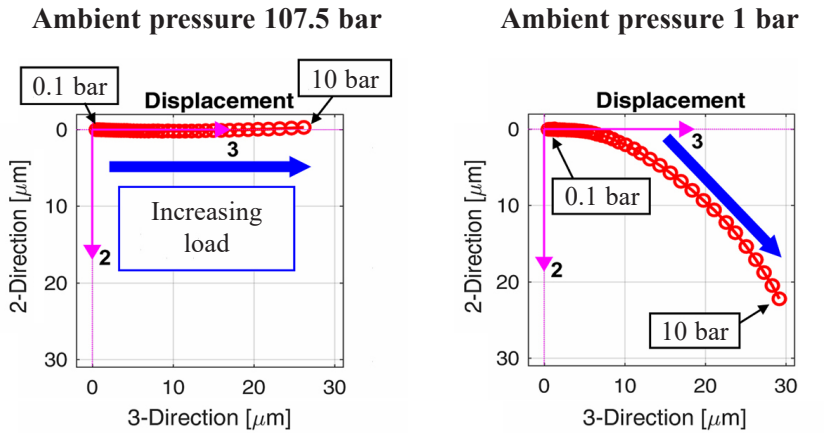

Fig. 16. Position of the shaft centreline for increasing bearing specific load

cavitation. With a specific bearing load of 10 bar, there is cavitation in the bearing at atmospheric pressure (white area on the oil ratio plot). The pressure peak is narrow in the circumferential direction and centered at about 15°, which is before the angular position of the shaft deflection at about 50° (see Fig. 16). This means the peak is before the narrowest gap in the bearing. Cavitation occurs in the upper part of the bearing from 90° to 270°, i.e. −90°.

In the pressurized bearing, there is no cavitation at all, the oil ratio is 1.0 everywhere. The region of cavitation at an atmospheric pressure now also contributes to carrying the load due to a pressure below the high ambient pressure. Due to the symmetry of the bearing, an increase in the pressure before the narrowest gap and a decrease after the narrowest gap must be symmetric to the horizontal 3-direction to obtain a resulting vertical force carrying the load. This can only be realized by a horizontal deflection.

As can be seen in Fig. 16, the deflection is more or less in a horizontal direction for the pressurized bearing (perpendicular to the bearing load), whereas for the bearing in atmospheric pressure it resembles the well-known Gümbel curve, i.e. with an increasing load, the component of the deflection in the load direction increases.

4. SINGLE-STAGE VERTICAL PUMP WITH CYLINDRICAL WATER-LUBRICATED BEARINGS

Fluid film bearings are normally linearized around their static load, which yields linear stiffness and damping coefficients. The linearized behavior can give good results in a wide range of dynamic loads if they do not exceed the static load. If the static load is zero or small, then the behavior is always nonlinear. A linear analysis does not show at which level the unstable system stabilizes (limit cycle). To get this result, which is essential for an assessment of the rotor behavior, a nonlinear analysis is necessary. In the following example, which is presented more in detail in [9], the rotor is unstable because it has unloaded cylindrical bearings.

4.1. Description of the model

The model of the vertical pump is shown in Fig. 17. The complete length of the assembly is about 12 m. The upper part and the motor are on the left side. The pump has only one impeller at the bottom shown on the right side. The pump rotor is shaded in blue. The casing of the pump, which is a pipe, is modelled as a shaft with zero speed. It is shaded in grey (partly visible as a black line). The pipe is fixed to a foundation, which is denoted as customer support in the model. It consists of a flange of the pipe. The flange is fixed with general springs to the ground. The general springs represent the stiffness of the foundation and introduce anisotropy to the system. The motor rotor is not modelled as part of the shaft since it is coupled to the pump shaft with a flexible coupling. The whole motor including its housing is modelled as a rigid mass (the sphere in Fig. 17) fixed to the flange at the customer support. The distance of the center of gravity to the support is bridged with a rigid element.

The pump shaft is supported in the pipe with an angular contact rolling element bearing, which also carries the axial load and several bush bearings. The rotor in the pipe is surrounded by pressurized water. Like in the previous example, the elevated ambient pressure and its influence on the cavitation are considered in the bearing analyses with a 2-phase model. The seal located at the impeller is also included in the analysis. Since the relative shaft vibration is relatively small at this location, linear coefficients can be used for the dominating modes. The coefficients are applied between the casing and the rotor.

The influence of the water located inside the pipe, which is displaced when the pipe vibrates, is considered by applying an added mass to the pipe (the mass of the enclosed water is added). The water mass displaced by the rotor has a small impact on the dynamics of the shaft line and has been neglected. The influence of the water outside the pipe was not considered.

4.2. Linear behavior, Campbell diagram

The Campbell diagram for a speed range up to 150% speed can be seen in Fig. 18.

The first two modes are a cantilever-like bending mode of the pipe and the rotor in two perpendicular directions. There is almost no relative displacement between the rotor and pipe. The next modes are bending modes of the rotor with increasing order and increasing relative displacement. The modes appear as elliptically forward and backward whirling modes. They are elliptic due to the anisotropy of the support stiffness. The forward modes with relative displacement become unstable (modes 4, 5, 7, and 9) when their frequency is below 50% of the speed, which is the whirling speed of the fluid in the cylindrical bearings.

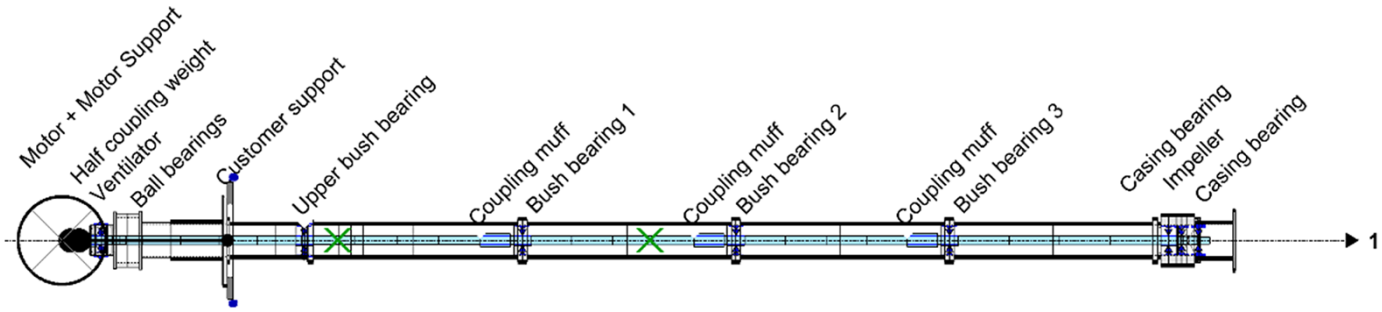

Fig. 17. Model of the vertical pump

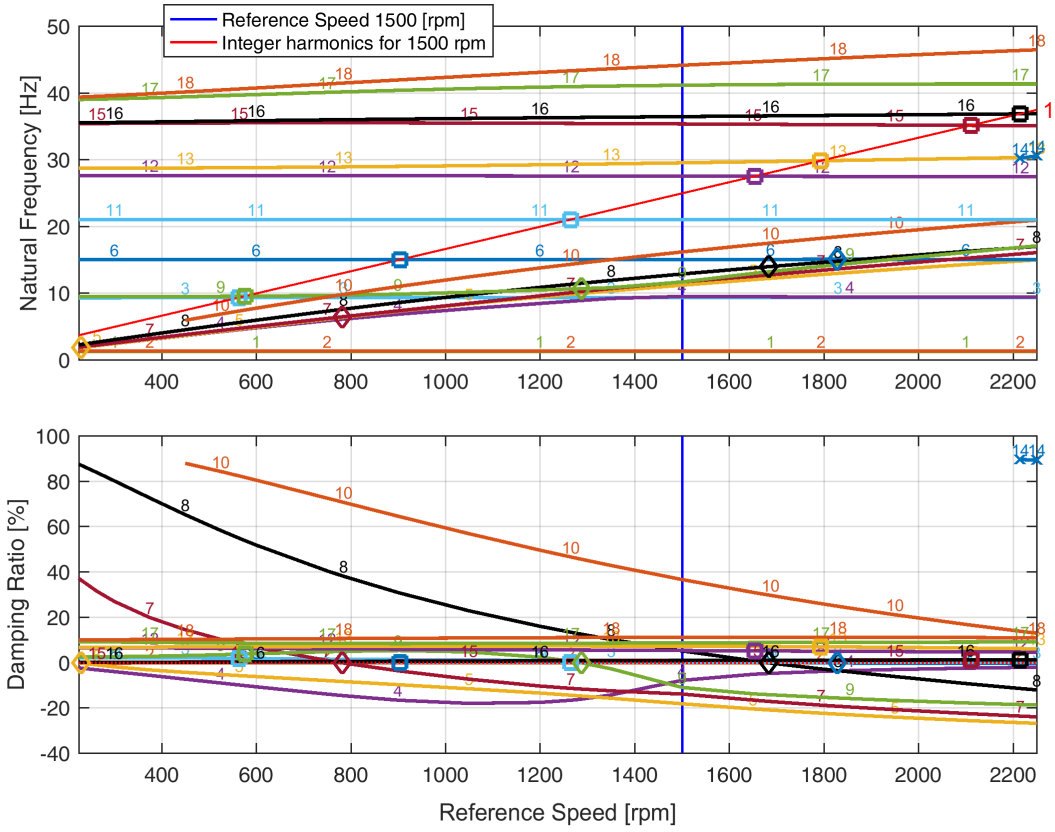

Fig. 18. Campbell diagram with eigenvalues

4.3. Results of a nonlinear run-up analysis

The nonlinear models of the fluid film bearings and the rolling element bearing, as well as the method used to solve the nonlinear equations, are presented in detail in [9]. For the present example, a run-up with an unbalance of G10 at the impeller has been conducted over a speed range from 10% to 110% speed in 60 s, which is almost stationary for this system.

Results of this analysis can be seen in the following figures: the absolute displacements of the pipe at the bearing locations in Fig. 19, the orbits of the relative displacements in the fluid bearings in Fig. 20, and the 3D shape at 1500 rpm in Fig. 21.

The vibrations of the pipe indeed are huge. At 100% speed (1500 rpm), the level at bush bearing 2 is several millimeters. The shape at about 1500 rpm in Fig. 21 corresponds to the

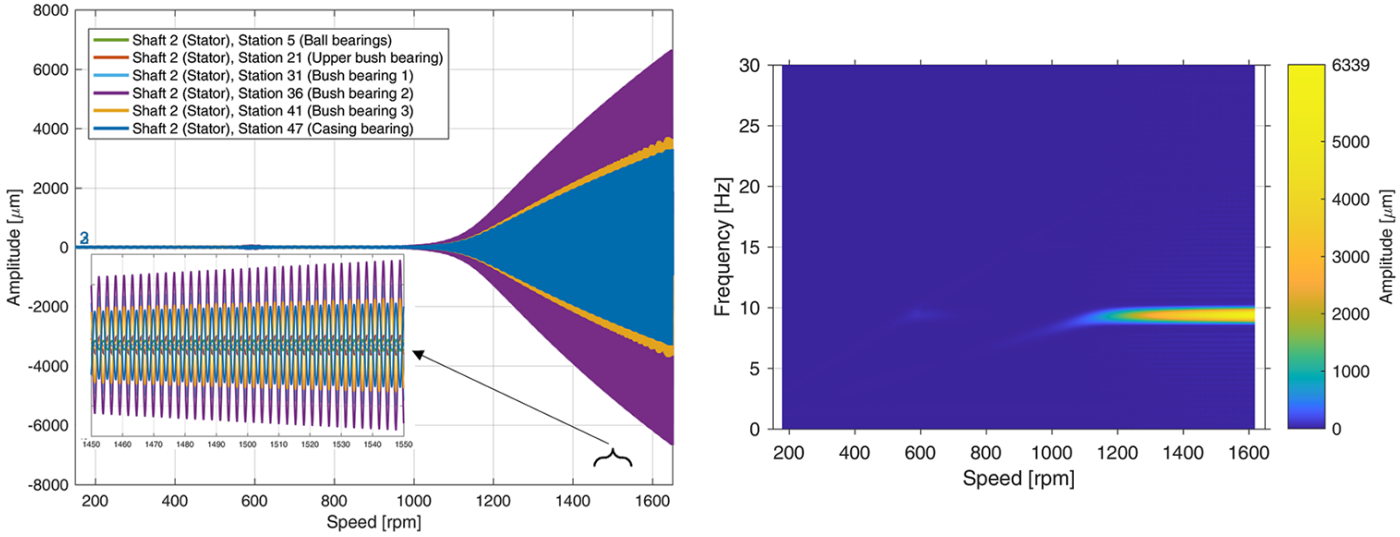

Fig. 19. Absolute vibrations of the pipe at the bearing locations

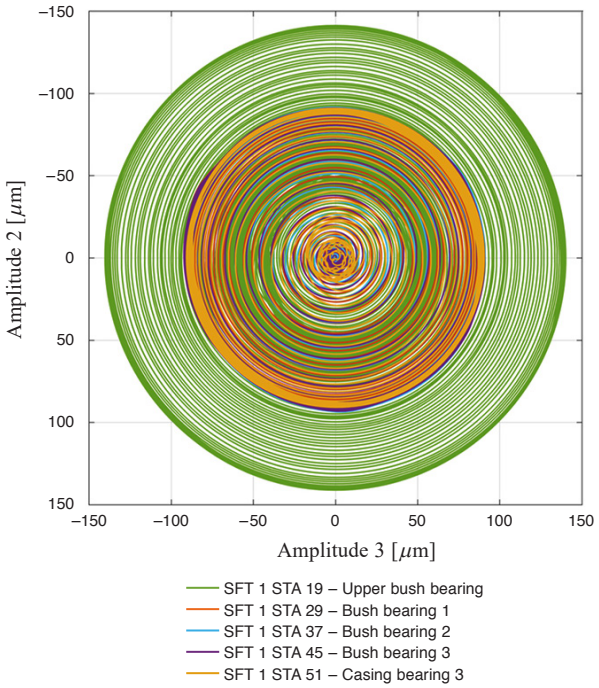

Fig. 20. Orbits of relative vibrations in the fluid bearings

2nd bending mode. By far the dominating frequency is about 10 Hz, which corresponds approximately to the frequency of this mode. The vibration level at the ball bearing at the top is much lower. At 1500 rpm, it is about 300 mm, which still corresponds to a high rms value of 33 mm/s. This is the location where the vibrations of such machines are typically measured. Other locations close to the bearings are difficult to access on such a pump.

The relative vibration level in the fluid bearings at nominal speed in Fig. 20 is about 90% of the bearing clearance for all bearings.

The force at nominal speed in bush bearing 2 is about 2400 N, corresponding to a specific dynamic load of 3 bar.

The vibration behavior of the pump as presented here is not acceptable or at least at the limit. The surrounding water, which is not considered in the analysis, probably helps to attenuate the vibration, especially at such levels as calculated here.

5. CONCLUSIONS

Three examples are presented demonstrating the requirements for rotordynamic analyses of pumps and typical results.

In the first example, the impact of seals on the static deflections and bearing loads as well as on the dynamic behavior is shown. Because of the seals, a simple rotor on 2 bearings turns into a statically overdetermined system.

The second example shows the behavior of the sector of a submerged pump. The special phenomenon that a higher specific bearing load does not lead to a more stable system is shown and explained.

A third example of a vertical pump with the rotor mounted in a pipe filled with water is shown. Limit cycles of the linearly unstable system during the run-up are calculated in nonlinear transient analysis.

REFERENCES

[1] D. Childs, *Turbomachinery Rotordynamics,* New York, Chichester, Brisbane, Toronto, Singapore: Wiley Inter Science Publication, 1993.

[2] J. Glienicke, “Feder- und Dämpfungskonstanten von Gleitlagern für Turbomaschinen und deren Einfluss auf das Schwingungsverhalten eines einfachen Rotors,” Dissertation, Technische Hochschule Karlsruhe, 1966.

[3] J. Lund and K. Thomsen, “A Calculation Method and Data for the Dynamic Coefficients of Oil Lubricated Journal Bearings,” in *Topics in Fluid Film Bearing and Rotor Bearing System Design and Optimization*. New York: ASME, 1978, pp. 1–28.

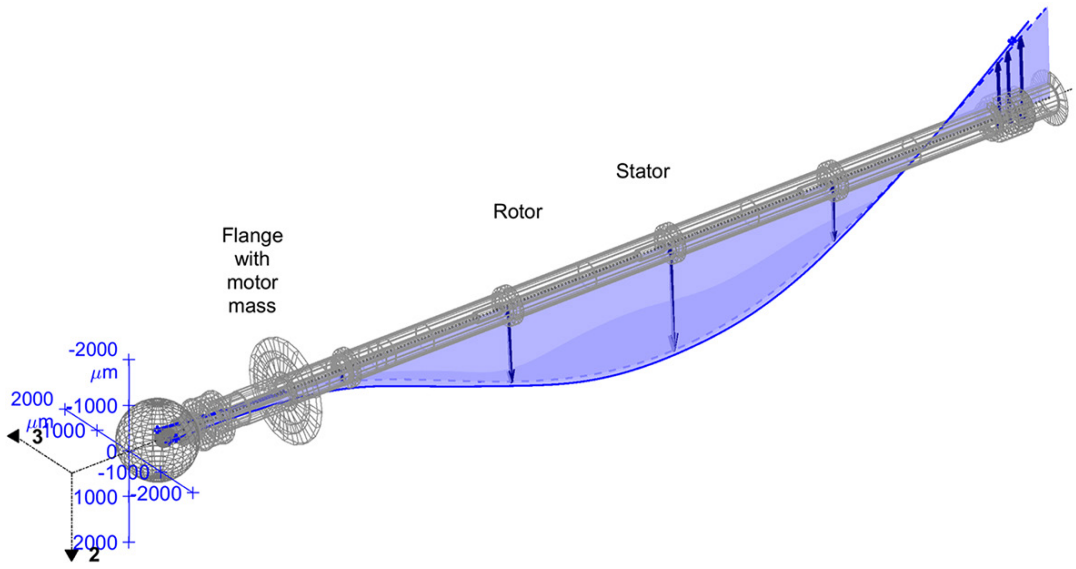

Fig. 21. Shape at nominal speed of 1500 rpm

[4] X. Cheng, "Einfluss einer Schmierfilmkavitation auf die dynamischen Eigenschaften von Quetschöldämpfern," Fortschr.-Ber. VDI Reihe 1 no. 243, Düsseldorf, VDI-Verlag.

[5] A. Fuchs, J. Schmied, and A. Kosenkov, "Hydrodynamic Bearings – State of the Art Calculations," in *Proceedings of the 11th Conference on Vibrations in Rotating Machines (SIRM)*, Magdeburg, Germany, 2015.

[6] R. Nordmann and F.J. Dietzen, "Calculating Rotordynamic Coefficients of Seals by Finite-Difference Techniques," *ASME J. Tribol.*, vol. 109, pp. 388–394, July 1987.

[7] J. Schmied, "Application of MADYN 2000 to rotor dynamic problems of industrial machinery," in *Proceedings of the 13th International Conference on Dynamics of Rotating Machines (SIRM)*, Copenhagen, Denmark, 2019.

[8] American Petroleum Institute, "Centrifugal Pumps for Petroleum, Petrochemical and Natural Gas Industries – ANSI/API Standard 610," Eleventh Edition, September 2010.

[9] J. Schmied and A. Fuchs, "Nonlinear Analyses in Rotordynamic Engineering," in *Proceedings of the 10th International Conference on Rotor Dynamics – IFToMM*, 2019, vol. 3, pp. 426–442.